energies

MDPI

Article

A Study on the Plasma Plume Expansion Dynamics of Nanosecond Laser Ablating Al/PTFE

Sheng Tan, Moge Wang *, Jianjun Wu *, Yu Zhang and Jian Li

College of Aerospace Science and Engineering, National University of Defense Technology, Changsha 410073, China; tansheng17@nudt.edu.cn (S.T.); zhangyu12@nudt.edu.cn (Y.Z.); lijian13c@nudt.edu.cn (J.L.)

* Correspondence: wangmoge@nudt.edu.cn (M.W.); jjwu@nudt.edu.cn (J.W.); Tel.: +86-0731-8457-5198 (M.W.); +86-0731-8457-5198 (J.W.)

Received: 25 May 2020; Accepted: 28 June 2020; Published: 29 June 2020

Abstract: To study the plasma plume expansion dynamics of nanosecond laser ablating Al/PTFE, the Al/PTFE propellant was prepared by a molding sintering method and the rapid expansion process of the plasma plume was photographed using fast photography technology. The effects of the proportion of Al, laser energy and ambient pressure on plasma plume expansion dynamics are analyzed. The results show that the plume expansion process of laser ablating Al/PTFE plasma can be divided into three stages and this phenomenon has not been reported in the literature. The Al powder doped in PTFE will block part of the laser transmission into the propellant, thus reducing the laser absorption depth of the propellant. In the case of short pulse laser ablation, the reaction rate between Al and PTFE is optimal when the reductant is slightly higher than the oxidant. As the laser energy increases, the light intensity of the plasma becomes stronger, the plasma size becomes larger and the existence time of plasma becomes longer. In the first stage plume, the plume expands freely at the ambient pressure of 0.005 Pa and the plume expansion distance is linearly related to time, while the shock wave formed at the interface between the plume front and the ambient gas at the ambient pressure of 5 Pa and the expansion can be described by S-T theory.

Keywords: laser-produced plasma; Al/PTFE; expansion dynamics; three stages expansion process; modified laser-assisted pulsed plasma thruster; fast photography

1. Introduction

In order to improve propulsion performance and system simplicities of conventional electric and laser propulsion systems, the concept of laser-electromagnetic hybrid propulsion system was proposed by Horisawa et al. [1–5]. A basic idea of these systems is that a bunch of laser-ablation plasma, induced by laser irradiation on a solid target, is additionally accelerated by electromagnetic field. Since the laser-ablation plasma has a directed initial velocity of tens of kilometers per second, which will be further accelerated by electromagnetic field, significantly high specific impulses could be expected. However, as one of the laser-electromagnetic hybrid propulsion systems, the laser-assisted pulsed plasma thruster (LAPPT) still needs to be improved. Firstly, because the propellant is exposed to the discharge channel, the late ablation still exists, which would limit the specific impulse and thrust efficiency [6]. At the same time, it makes the single ablation mass of the propellant uncontrollable. Secondly, the propellant must be electrical insulating materials, which limits the range of propellant selection.

In order to improve the propulsion performance of the LAPPT, some modifications have been made to the LAPPT by Zhang [7,8], and a schematic diagram of the modified laser-assisted pulsed plasma thruster (MLAPPT) is shown in Figure 1. By using ceramic tubes to isolate the propellant from the discharge channel, discharge arc cannot ablate the propellant. So it is able to avoid the occurrence of late ablation. At the same time, it also makes conductive materials be alternative materials

for the propellant, which means that it can use any condensed matter as the propellant like laser propulsion [9]. Therefore, the selection of propellant for MLAPPT can refer to the related research work of laser propulsion.

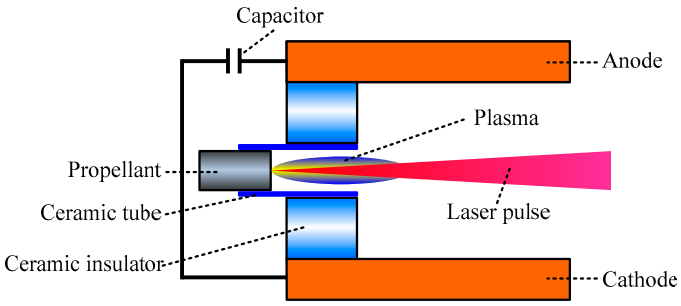

Figure 1. Schematic diagram of modified laser-assisted pulsed plasma thruster.

The study of laser propulsion [10,11] shows that polymers have higher impulse coupling coefficients and lower specific impulses, while metals have higher specific impulses and lower impulse coupling coefficients. Therefore, in order to combine the advantages of polymers and metals, researchers have doped polymers with metal powders in order to obtain higher propulsion performance. Schall et al. [10] studied the propulsion performance of polyoxymethylene (POM) doped with Al and Mg powder, and the results showed that the addition of metal powder can reduce the propulsion performance. The possible reason is that the laser pulse is too long, making the ablation plume shield too much laser energy, so it is recommended that the laser pulse must be an order of magnitude shorter or more. Cheng et al. [12] doped metal powder of different types and diameters in polyvinyl chloride (PVC), and the experimental results showed that the addition of metal can effectively improve the specific impulse. Peng et al. [13] doped Al and Fe powder in the POM and measured their propulsion performance, and the results showed that metal powder can improve the propulsion performance of propellant under certain conditions.

Polytetrafluoroethylene (PTFE) is an alternative propellant for laser thrusters [10,14], pulsed plasma thrusters (PPT) [15,16] and MLAPPT [8,17] due to its excellent thermal stability, electrical insulation and stability under low pressure [8,18]. In particular, PTFE was the only propellant used for PPT space applications [19]. However, the ablation efficiency of PTFE induced by nanosecond lasers is not high due to the weak laser absorption characteristics and the high bond energies of the PTFE [20,21]. It is necessary to modify the PTFE to improve its performance when it is applied to the MLAPPT as propellant. In this paper, Al was used as the dopant of PTFE to make composite propellants to explore high-quality propellants for MLAPPT. The reasons for choosing Al are mainly the following three points. Firstly, as a kind of metal, Al absorbs laser energy by surface absorption. Therefore, doping Al into PTFE is expected to reduce the laser penetration depth, which can increase the laser energy per unit volume and improve the ablation efficiency of the propellant. Secondly, the ionization energy of the Al is lower, which is easier to be ablated and ionized by laser. Last but not the least, at high temperatures (above 500 °C) or at high impact velocities (greater than 300 m/s), PTFE will dissociate into small molecule fluorocarbon gases. These gases have high activity and can react exothermically with Al (to produce aluminum fluoride and carbon). The calorific value of the reaction is about 8.53 kJ/g (calorific value is twice that of TNT (4.18 kJ/g)) [22].

The working process of MLAPPT can be divided into two stages: laser ablation to generate plasma and discharge acceleration. The laser ablation plasma dynamics of the first stage has a great impact on the discharge acceleration of the second stage. Therefore, deepening the understanding of the laser plasma dynamics of the first stage is crucial to the understanding of the working process of the LAPPT. At the same time, doping polymers has been widely used to explore new ablation phenomena and ablation mechanism. Therefore, studying the ablation plasma dynamics of Al/PTFE can also explore new ablation phenomena and ablation mechanism.

In this paper, the Al/PTFE propellant with different mass ratios was made by molding sintering method. The plasma evolution process of nanosecond pulse laser ablation of Al/PTFE propellant under different ambient pressures and different laser energies was photographed by the ultrahigh speed camera. Then, the plasma evolution process was analyzed, and the data was extracted from the plasma image to study the plasma expansion dynamics.

2. Experiments

2.1. Preparation of Propellant

The main materials used include Al powder (average diameter of 5~6 μm, from Changsha Tianjiu Metal Material Co., Ltd., Changsha, China), PTFE (average diameter of 25 μm, from Minnesota Mining and Manufacturing Co., Sao Paulo, USA), and silane coupling agent (KH-560, from Kangjin New Material Technology Co., Ltd., Dongguan, China). The preparation process of propellant is shown in Figure 2, and the steps are as follows:

(1) Modification of Al powder. Firstly, 50 g Al powder was added to 120 mL of absolute ethanol and 30 mL of deionized water, and then 5 g of KH-560 was added. After that, the mixture was dispersed by high shear dispersion emulsifier for 10 min to obtain the solid-liquid mixture. Secondly, the solid-liquid mixture was magnetically stirred at 70 °C water bath for 5 h. Thirdly, the solid-liquid mixture was suction filtered and washed with absolute ethanol during the suction filtration process. The filter cake was put into a vacuum drying box and dried at the temperature of 60 °C for 24 h. Finally, the dried filter cake was milled to obtain the modified Al powder.

(2) Mixing and drying. Firstly, weighed a certain amount of modified Al powder and PTFE powder and immersed them in absolute ethanol. After that, the mixture was dispersed with the high shear dispersion emulsifier for 10 min and then mechanically stirred with an electric mixer for 2 h to obtain the solid-liquid mixture. In the next step, the solid-liquid mixture was suction filtered. Subsequently, the filter cake was put into a vacuum drying box and dried at the temperature of 60 °C for 24 h. Finally, the dried filter cake was milled to obtain the mix powder.

(3) Molding and sintering. Firstly, filled the mixed powder into the molding mold, and then pressurized the mold with the powder compressing machine to obtain the pressurized propellant. In order to eliminate the internal pressure of the pressurized propellant and prevent from cracking of the pressurized propellant caused by internal pressure during sintering, it is necessary for the pressurized propellant to standing for 24 h before sintering. Then, the tube furnace was used to sinter the pressurized propellant. Before sintering, the tube furnace was vacuumed and then continuously filled with argon gas as a protective gas until the sintering was completed. The temperature control procedure during sintering [22] is shown in Figure 3. Finally, Al/PTFE propellant was obtained.

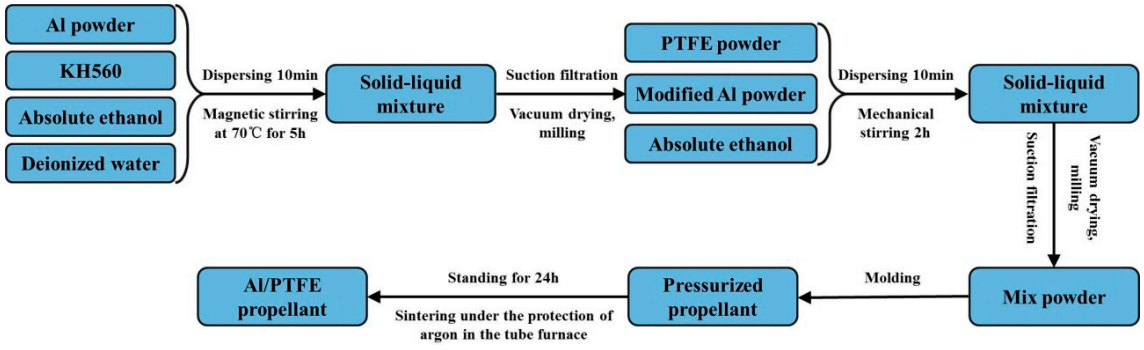

Figure 2. The preparation process of Al/PTFE propellant.

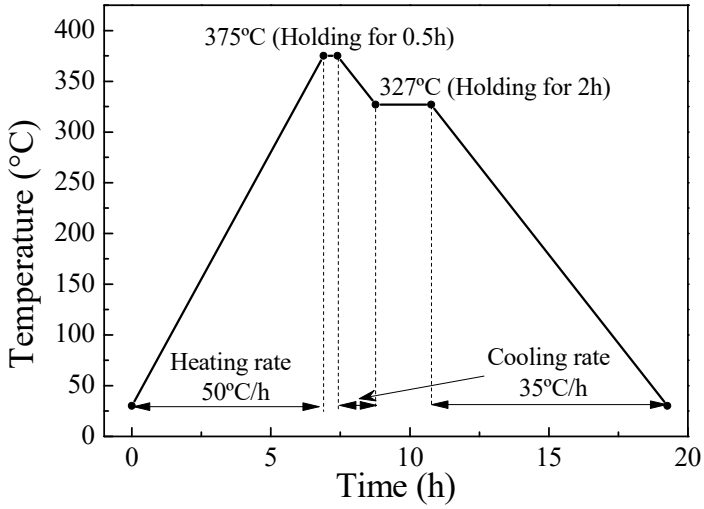

Figure 3. The temperature control procedure during sintering.

2.2. Laser Ablation Experiment System

The schematic of the experimental setup is given in Figure 4. The laser beam is produced by a Nd:YAG laser (Beamtech Optronics Co., Ltd., Beijing, China) with a pulse width of 8 ns (full-width at half-maximum, FWHM) and a wavelength of 1064 nm. The maximum energy of the laser is about 900 mJ, and the laser energy output can be controlled by adjusting the energy attenuator located at the laser head. The laser is focused on the propellant by a focusing lens with 400 mm focal length. The propellant and focusing lens are installed in the vacuum chamber. The ultra-high speed camera used here is the XXRapidFrame multichannel ICCD camera system (Paul Hoess KG/Stanford Computer Optics, Inc., Munich, Germany), equipped with an internal delay generator. A digital delay pulse generator (DG535, Stanford Research Systems, Sunnyvale, USA) was used to generate the pulse signal to trigger the laser and the camera system, respectively. 4Spec, the original software of the camera system, was used to collect the images.

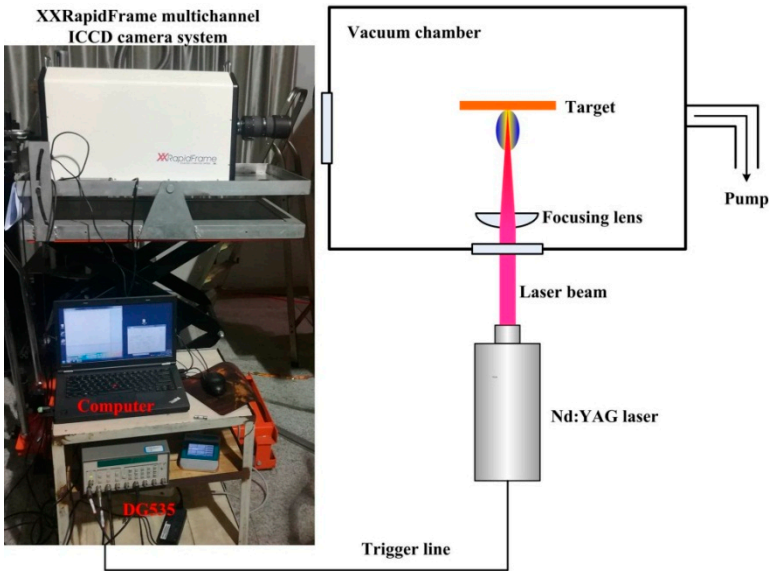

Figure 4. Schematic of the experimental setup.

In the experiment, the exposure time of the camera system was set to 10 ns, which can effectively freeze the motion of the plasma plume (when the expansion velocity is 50 mm/μs, the moving distance in the exposure time is only 0.5 mm) to obtain the spatial distribution of the plasma. The exposure

time was kept constant under different experimental conditions to compare the plasma plume among different experimental conditions. In order to improve the visibility of the plasma plume images, grey images were converted into pseudo-color images using 4Spec software.

3. Results and Discussions

3.1. Plasma Plume of Laser Ablating Al/PTFE

The plasma plume evolution process of 26.5% Al at a background pressure 0.005 Pa and laser energy of 542.3 mJ is shown in Figure 5, where it can be seen that the laser ablation plasma plume is almost symmetrically distributed with respect to the normal direction of the propellant.

After laser irradiation of the propellant surface, the laser evaporates or even ionizes the propellant to form a plasma plume above the propellant surface when the laser intensity exceeds the ablation threshold of the propellant. If the plasma plume appears and starts to expand outward and the laser pulse does not end, the plasma will absorb part of the laser energy and reduce the laser energy reaching the propellant surface, that is, the plasma shielding occurs. The interaction between the laser and the plasma will further heat and ionize the plasma, thereby further improve the internal energy of the plasma. It can be seen from Figure 5 that a relatively strong luminescence phenomenon can be seen in the plasma plume at 0.05 μs, which may be due to the intense radiation generated by the interaction between the laser and the plasma.

Because the laser plasma plume expands at a lower ambient pressure and the initial pressure of the plasma is much higher than the ambient pressure, the plasma plume expands freely with little external viscous force. The vertical displacement (i.e., the direction parallel to the surface of the propellant) of the plasma plume is smaller than the lateral displacement (i.e., the displacement in the opposite direction of the laser incidence) and the velocity of vertical displacement motion is smaller (the average velocity from 0.20 μs to 0.50 μs is about 9.461 mm/μs). This is because the pressure gradient in the direction with a smaller initial plume size is greater [23], and its lateral dimension (ablation depth) is much smaller than the vertical dimension (laser radius). Therefore, the lateral pressure gradient is larger and the expansion velocity is faster (the average velocity from 0.20 μs to 0.50 μs is about 69.383 mm/μs), which makes the plume quickly become longer in the lateral direction.

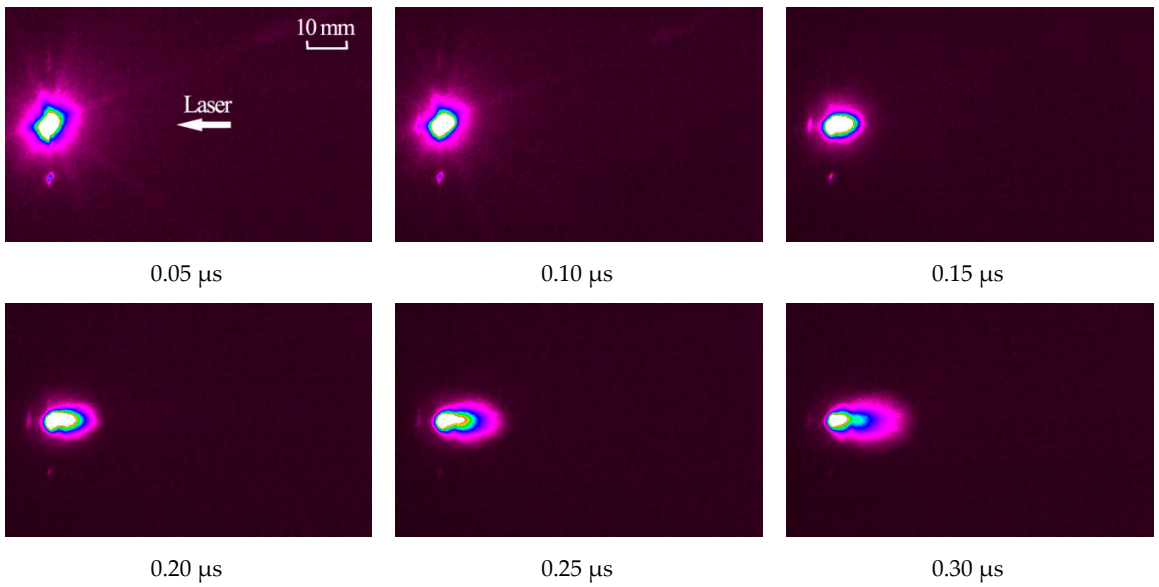

Figure 5. *Cont.*

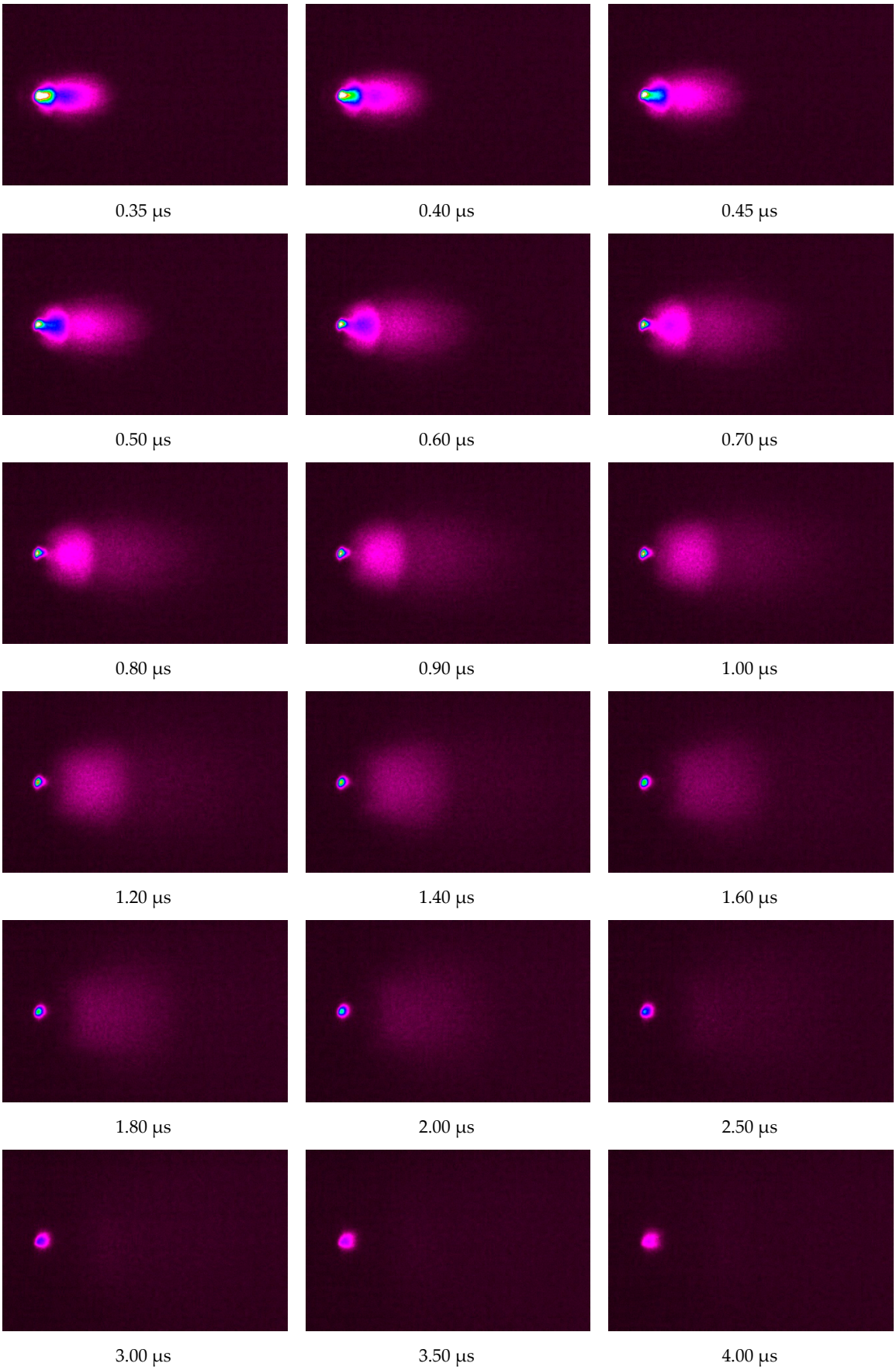

Figure 5. *Cont.*

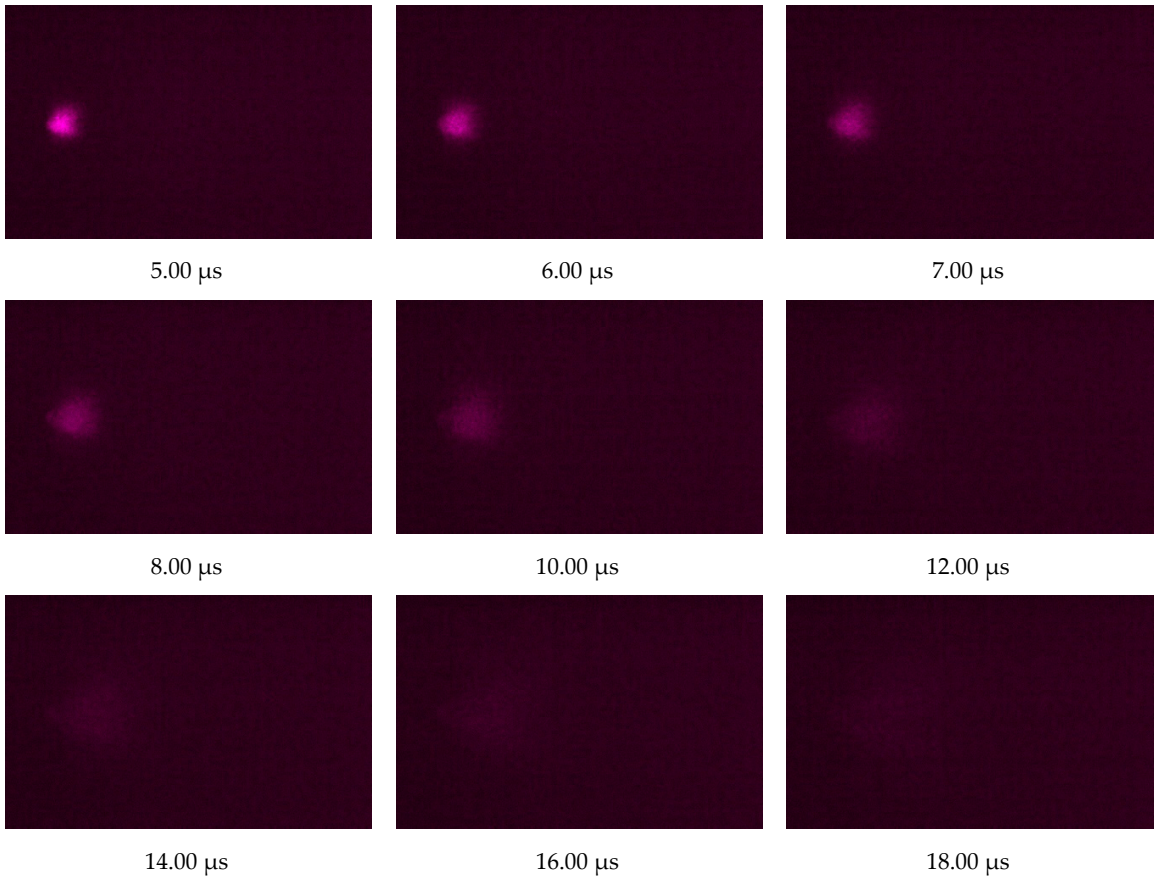

Figure 5. The plasma plume evolution process of 26.5% Al at ambient pressure 0.005 Pa and laser energy 542.3 mJ.

On the one hand, the plasma temperature will decrease over time because the expansion of the plasma plume after the end of the pulsed laser is adiabatic [24]. On the other hand, the electron number density will decrease rapidly with the rapid expansion of the plasma and the probability of electron collision ionization will decrease. The two factors lead to the decrease of the core bright area of the plasma plume (white area in the plume) over time. At the same time, these also lead to the outward expansion of the plume experiencing a process from highlight to gradually fading away. It is worth noting that even if it is up to the time of 2.00 μs, there is still a higher intensity of light emission in the region near the ablation position of the propellant surface, and the emission region is almost fixed on the propellant surface. This region may be due to the collision of particles in the high pressure zone of the initial expansion plume, thus forming a Knudsen layer that stays on the surface of the propellant [25].

At the time of 0.50 μs, the light emission in the middle of the plume can be clearly seen to be stratified, that is, the light intensity of the plume on the right side of the plume is low (it is defined as the first stage plume in this article) and the light intensity on the left side of the plume is higher (it is defined as the second stage plume in this article), and at this time the plume appears "gourd-like" shape. Because the first ionization energy of Al is low (5.986 eV), and the first ionization energies of C (11.26 eV) and F (17.422 eV) are high, Al is more easily ionized when absorbing the same photon energy. At the same time, when PTFE is irradiated with laser light, part of the photon energy will be used to break the chemical bond and produce a variety of small molecule products, and then the small molecule products continue to absorb the photon energy and are ionized into plasma [26]. Therefore, compared to PTFE, Al is more easily ablated. Al is first ablated away from the propellant surface and then ionized and accelerated by absorbing photon energy when it expands outward, so its movement speed will be faster than that of PTFE which is ablated and ionized later. Therefore, the first stage plume may mainly contain aluminum ions due to the ions mainly contained in the fast structure of the plume [27].

The light intensity of the first stage plume gradually decreases and disappears after 0.50 μs, which results in the position of the plume front being difficult to measure after 0.50 μs. The plume within 0.20 μs is not easy to measure either due to the strong light emission caused by the interaction of the incident laser and plasma. Therefore, the expansion velocity of the first stage plume front is calculated from the position of the plume front in the time of 0.20 μs~0.50 μs. From the change trend of the plume length of the first stage over time in Figure 6, it can be seen that the plume length of the first stage increases linearly over time, and the expansion rate is about 69.594 mm/μs obtained by fitting the formula $L_p = a_1 t$.

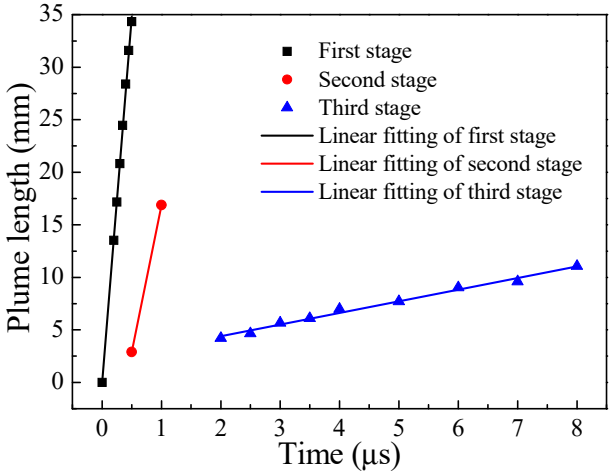

Figure 6. The plasma length of three stages changes with time at ambient pressure 0.005 Pa and laser energy 542.3 mJ.

At the time of 0.50 μs~2.50 μs, the second stage plume gradually expands and disappears with as time evolvesd During this period, the overall shape of the visible region of the plume changes from a "gourd-like" shape to a "fan" shape and finally to a "circular" shape near the surface of the propellant. Because the plume front of the second stage is fuzzy and it is difficult to obtain its front position with the program, the estimated positions of the two time points (0.50 μs and 1.00 μs) are obtained manually (as shown in Figure 6). The average velocity of the plume expansion in the second stage from 0.50 μs to 1.00 μs is about 27.948 mm/μs. The second stage plume expansion speed is lower than the first stage plume may be because the second stage plume expands in the subsequent flow field of the first stage plume, which is equivalent to the second stage plume moving in the background gas with a certain pressure. Therefore, the second stage plume will collide with the first stage tail plume, which leads to the lower expansion velocity of the second stage plume. At the same time, the obvious contact edge between the first stage plume and the second stage plume may represent the formation of the shock wave, which is similar to the shock wave formed by the laser plasma moving in the background gas with a certain pressure [28].

It can be seen from the image of 2.00 μs~18.00 μs in the Figure 5 that after the first stage plume and second stage plume almost disappears, a new plume appears in the region near the surface of the propellant (which is defined as the third stage plume in this paper). It can be seen from the relationship between the plume length of the third stage and time in Figure 6 that the expansion velocity of the third stage plume is low and the linear fitting results in a velocity of about 1.110 mm/μs, which is much lower than the expansion velocity of the first stage plume and the second stage plume. At the same time, because the process occurs about 2 μs after the end of the laser and the first stage plume and the second stage plume have almost disappeared at this time, the third stage plume may be formed by the chemical reaction of Al and PTFE.

The total plume area and the third stage plume area are shown in Figure 7. The area of the third stage plume is obtained by intercepting a part of the image from the overall plume image which is

close to the third stage plume to reduce the influence of the plumes in the first stage and the second stage. It can be seen from Figure 7 that with the increase of time, the total area of the plume increases first and then decreases, then increases with the emergence of the third stage plume and eventually decreases. The linear fitting of the total plume area within the time of 0.00 μs~0.50 μs shows that the total area of initial plume is linearly related to time, and the growth rate of the total area of initial plume is about 724.101 mm^2/μs. The plume area of the third stage increases first and then decreases with the increase of time, which reflects the expansion and fading of the third stage plume.

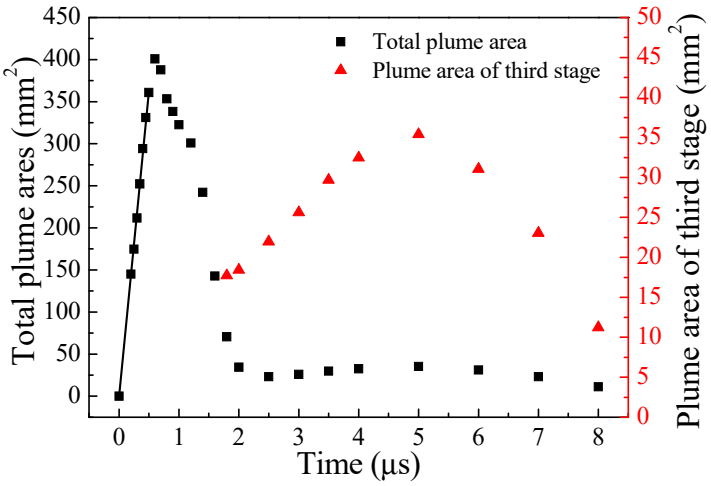

Figure 7. The variation of the total plume area and the third stage plume area with time at ambient pressure 0.005 Pa and laser energy 542.3 mJ.

3.2. The Effect of Al Proportion

Figure 8 shows the evolution process of laser ablation plume for different proportions of Al. At the time of 0.05 μs, there is a big difference in the plume intensity and area under different Al proportions. Since the laser energy density is the same, the possible reason for this phenomenon is that the space distributions of laser energy in different proportions of propellant are quite different. PTFE absorbs laser energy by volume absorption (the laser absorption depth of the propellant exceeds the heat diffusion depth, and more laser energy is transmitted into the propellant) and Al absorbs the laser energy by surface absorption (the laser absorption depth of the propellant is smaller than the heat diffusion depth, and the laser energy is mainly absorbed in the smaller region near the surface of the propellant). Al powder doped in PTFE will block part of the laser transmission into the propellant, thus reducing the laser absorption depth of the propellant. Therefore, the laser energy absorption of the propellant has a tendency to change from volume absorption to surface absorption. With the increase of Al proportion doping in the PTFE, the absorption depth of the propellant decreases and the surface temperature of the propellant heats up faster. The earlier the plasma is formed, the easier it is to form strong radiation of the interaction between the laser and the plasma.

At the time of 0.20 μs~10.0 μs, the overall development of laser ablation plume with different Al proportions was similar and all experienced the development of the first, second and third stage plume. The development of the first stage plume and the second stage plume was similar, except that the expansion velocity of the plume front in the first stage increases with the increase of Al proportion which will be analyzed in detail in the later comparison of the plume data. It can be seen from the comparison of plume images of 2.00 μs~10.0 μs at different Al proportions in Figure 8 that there is a great difference in the third stage plume and the light intensity of the third stage plume increases first and then decreases with the increase of Al proportion.

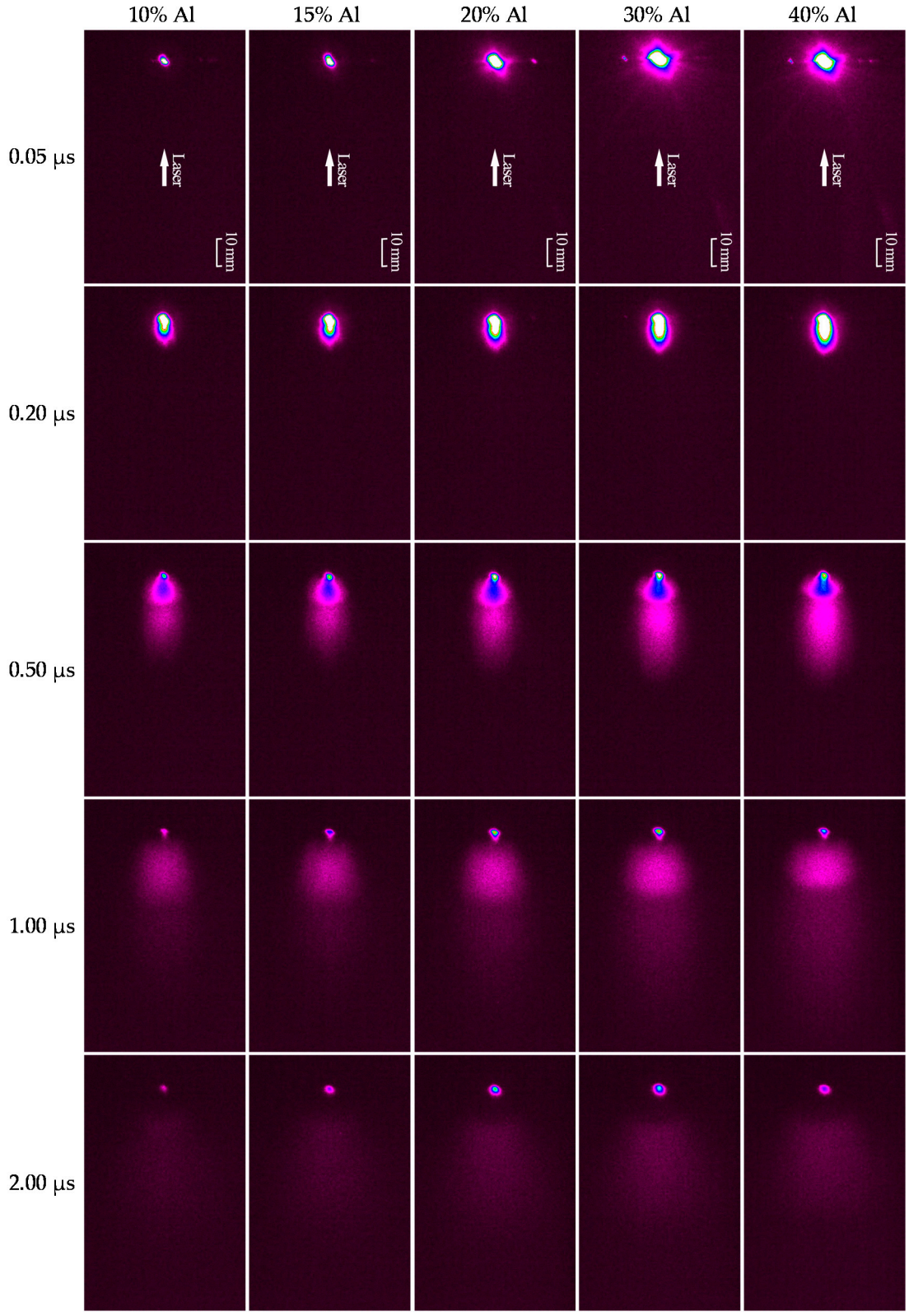

Figure 8. *Cont.*

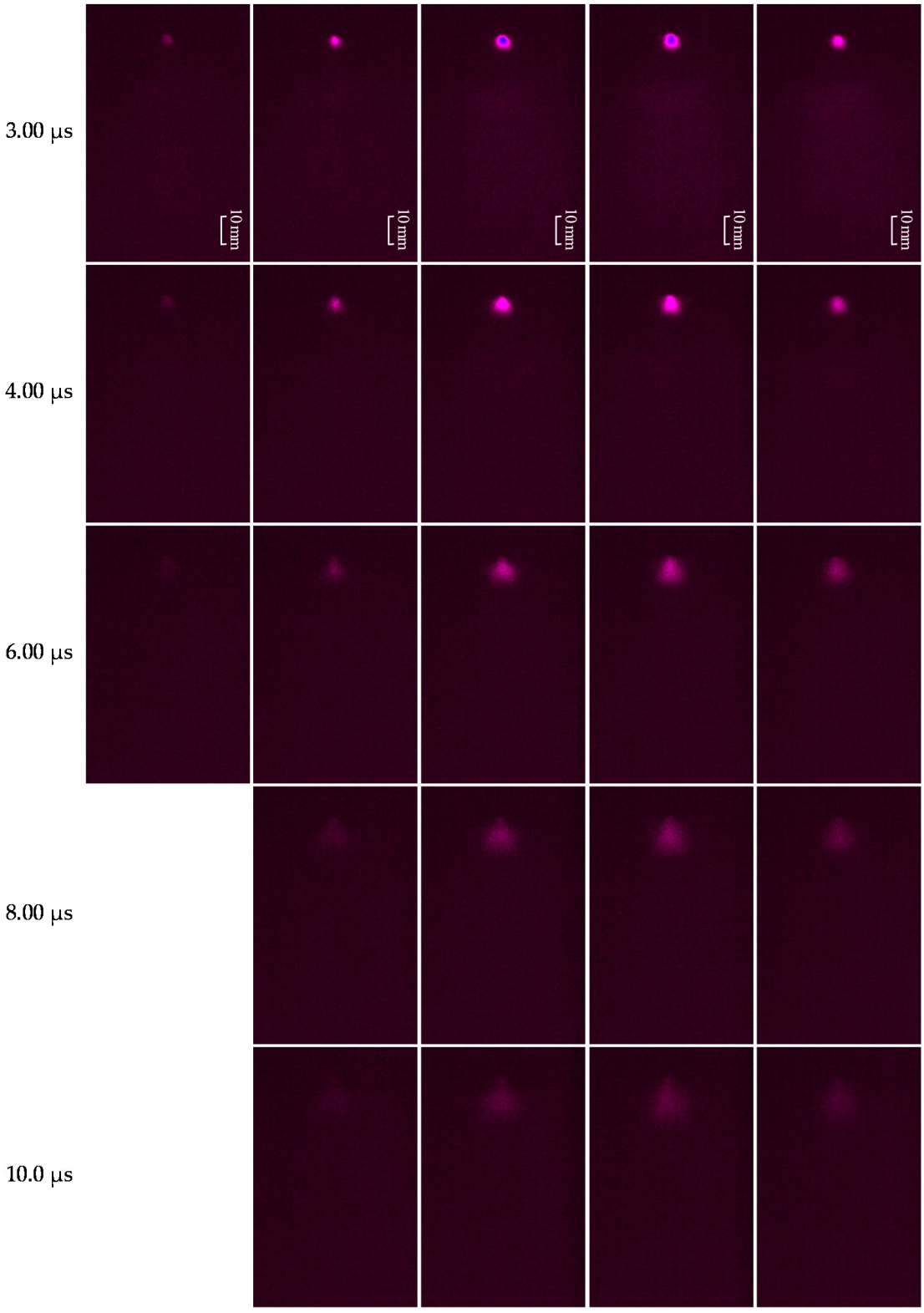

Figure 8. The evolution process of laser ablation plume at different proportions of Al (ambient pressure 0.005 Pa and laser energy 542.3 mJ).

The plume length of the first stage variation with time and its linear fitting at different proportions of Al are shown in Figure 9. It can be seen from the figure that the plume length of the first stage has a linear relationship with time and the slope of the linear fitting increases with the increase of

Al proportion which indicates that the plume expansion velocity increases. The expansion velocity increases from 58.036 mm/μs at 10% Al to 74.609 mm/μs at 40% Al. The main reason for this phenomenon is that more laser energy is concentrated on the surface layer of the propellant with the increase of Al proportion, which accelerates the first stage plume more strongly.

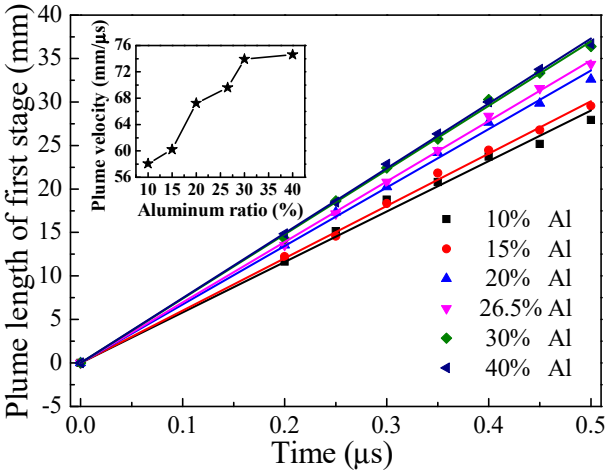

Figure 9. The plume length of the first stage variation with time and its linear fitting at different proportions of Al (ambient pressure 0.005 Pa and laser energy 542.3 mJ).

The total plume area variations with time at different proportions of Al are shown in Figure 10. It can be seen from the figure that the change trends of the total plume area at different proportions are the same: with the increase of time, the total plume area increases first and then decreases, then slightly rises and finally continues to decrease. From the distance between the different curves in the time of 0.00 μs~2.00 μs in Figure 10, we can see that the distance between the 15% Al and 20% Al is the largest, which indicates that the influence on plume area is the greatest when the Al proportion changes between these two proportions. The plume area within 0.00 μs~0.50 μs is analyzed separately, the total area of initial plume variation with time and its linear fitting at different proportions of Al are shown in Figure 11. It can be seen from the figure that the total area of initial plume has a linear relationship with time and the growth velocity of the initial plume area increases from 464.927 mm^2/μs at 10% Al to 817.979 mm^2/μs at 40% Al.

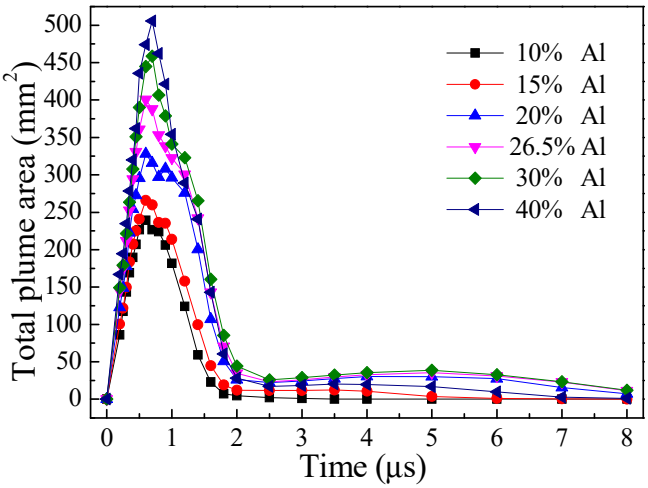

Figure 10. The total plume area variation with time at different proportions of Al (ambient pressure 0.005 Pa and laser energy 542.3 mJ).

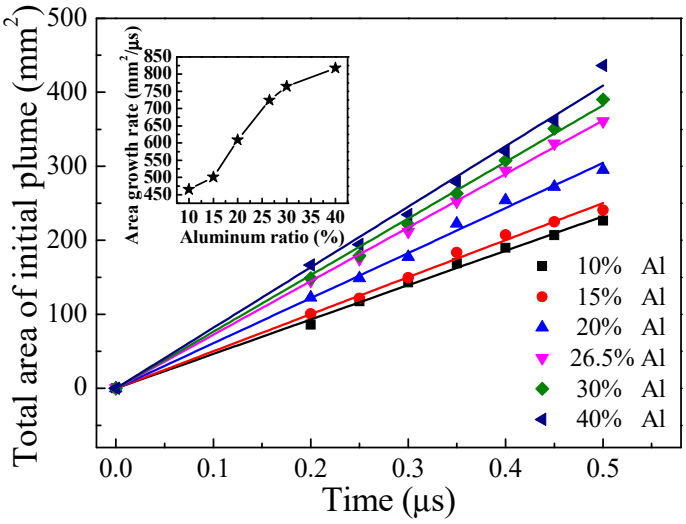

Figure 11. The total area of initial plume variation with time and its linear fitting at different proportions of Al (ambient pressure 0.005 Pa and laser energy 542.3 mJ).

The change of plume area in the third stage over time under different Al proportions is shown in Figure 12, it can be seen from the figure that the overall change trends of plume area under different Al proportions are the same: increase first and then decrease over time. Meanwhile, it can be found that the maximum area of plume in the third stage increases first and then decreases with the increase of Al proportion and the maximum areas are sorted as follows: 30% Al > 26.5% Al > 20% Al > 40% Al > 15% Al > 10% Al. The plume length of third stage variation with time and its linear fitting at different proportions of Al are shown in Figure 13. It should be noted that the plume will gradually disappear with the expansion of the third stage plume, which will lead to the plume front position decrease in the later stage of plume expansion, so the Figure 13 only shows the plume front position when the plume is strong. It can be seen from Figure 13 that the slope of linear fitting (i.e., expansion velocity) increases first and then decreases with the increase of Al proportion and the expansion velocities are sorted as follows: 30% Al > 26.5% Al > 20% Al > 40% Al > 15% Al > 10% Al. This sorting is the same as the plume maximum area sorting in the third stage. Because the third stage plume is generated by the reaction of Al and PTFE induced by the high temperature on the propellant surface after laser ablation, it can be further speculated that the reaction rate between Al and PTFE is optimal when the reductant is slightly higher than the oxidant in the case of short pulse laser ablation.

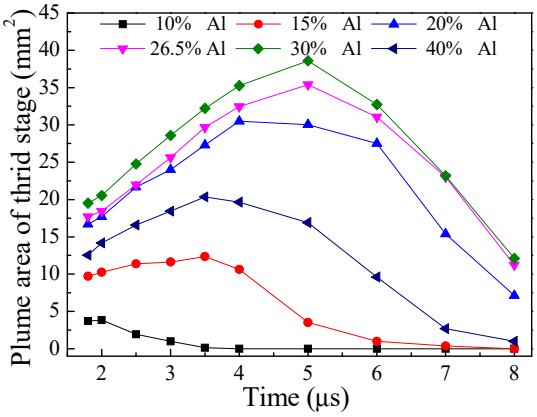

Figure 12. The plume area of third stage variation with time at different proportions of Al (ambient pressure 0.005 Pa and laser energy 542.3 mJ).

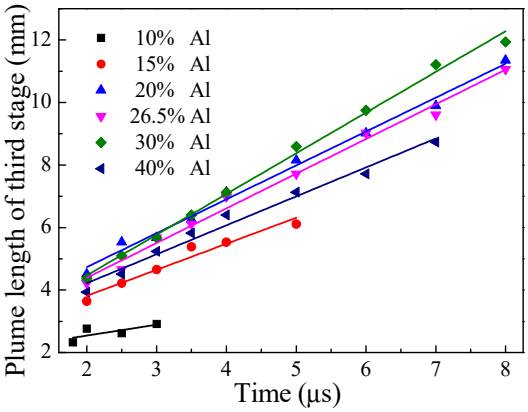

Figure 13. The plume length of third stage variation with time and its linear fitting at different proportions of Al (ambient pressure 0.005 Pa and laser energy 542.3 mJ).

3.3. The Effect of Laser Energy

The evolution process of laser ablation plume at different laser energy is shown in Figure 14. It should be noted that the stratification times of the first stage plume and the second stage plume are advanced when the laser energy is 260.4 mJ, so a 0.35 μs plume image is added. Comparing the plasma evolution process at different laser energies in Figures 5 and 14, we can see that the development of the laser ablation plume has gone through three stages, but it varies in morphology, especially at lower laser energy.

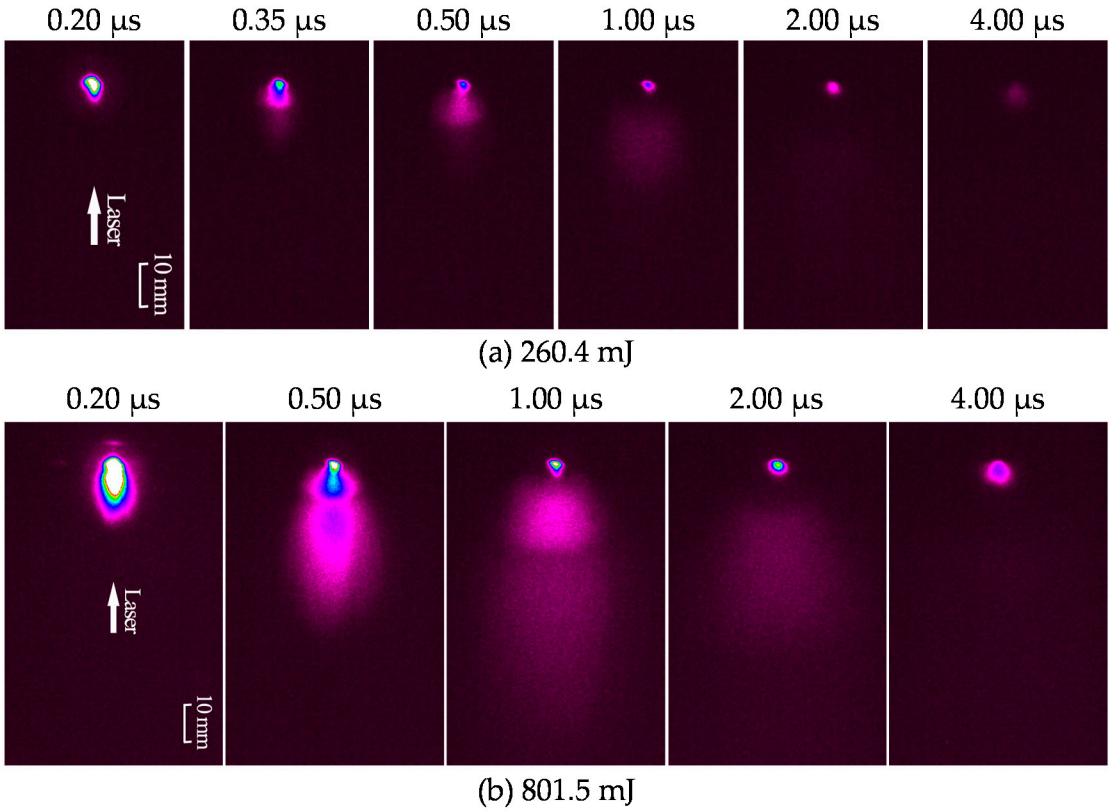

Figure 14. The evolution process of laser ablation plume at different laser energy (ambient pressure 0.005 Pa and 26.5% Al).

At lower energy (260.4 mJ), the light intensity of the plasma is weak, the plasma size is small and the plasma is fast to disappear. At this time, the first stage plume radiation is so weak that the first stage plume has almost disappeared at the beginning of the second stage plume development (as shown in

0.35 μs in Figure 14a), which indicates that the ionization degree of the first stage plume is low. As the laser energy increases, the light intensity of the plasma becomes stronger, the plasma size becomes larger and the existence time of plasma becomes longer. This may be caused by two reasons. On the one hand, the mass ablation rate increases with the increase of the laser energy, thereby increasing the number density of excited particle. On the other hand, the shielding effect of the plasma on the laser increases with the increase of the laser energy, which makes the plasma absorb more energy through the interaction with the laser, thereby increasing the ionization rate of the plasma and number density of excited particles [29]. At the same time, the light intensity of the third stage plume increases with the increase of laser energy.

The plume length of first stage variation with time and its linear fitting at different energies are shown in Figure 15, it can be seen from the figure that the expansion velocity of the first stage plume increases with the increase of laser energy and the expansion velocity increases from 21.430 mm/μs at 260.4 mJ to 88.678 mm/μs at 801.5 mJ. The main reason for this phenomenon is that the ionization time and expansion time of the propellant are shortened with the increase of laser energy and the plasma absorbs more energy after the interaction between the plasma and the laser, so the plasma obtains more kinetic energy.

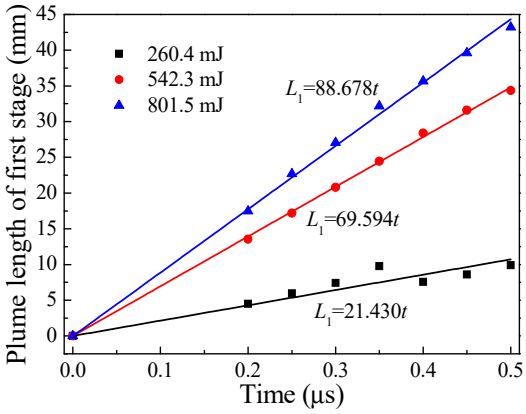

Figure 15. The plume length of first stage variation with time and its linear fitting at different energies (ambient pressure 0.005 Pa and 26.5% Al).

Figure 16 shows the variations of total plume area over time at different energies. From the figure, we can see that the change trends of the total plume area are the same: with the increase of time, it increases first and then decreases, then slightly rises and finally continues to decrease. At any time, the total plume area of the higher laser energy is always larger than that of lower laser energy which means that the plasma space size increases as the laser energy increases. The straight line in Figure 16 is a linear fitting of the total plume area in the time of 0.00 μs~0.50 μs, and it can be seen that the growth rate of the total initial plume area increases with the increase of laser energy.

The third stage plume area variations with time at different laser energies are shown in Figure 17. It can be seen from the figure that plume area of the third stage increases first and then decreases over time, and the plume area of the third stage increases with the increase of laser energy. Figure 18 shows the variation of the third stage plume lengths over time at different energies, and it can be seen from the figure that the expansion velocity of the third stage plume increases with the increase of laser energy. The results of plume area and expansion velocity of the third stage plume show that the reaction rate between Al and PTFE increases with the increase of laser energy.

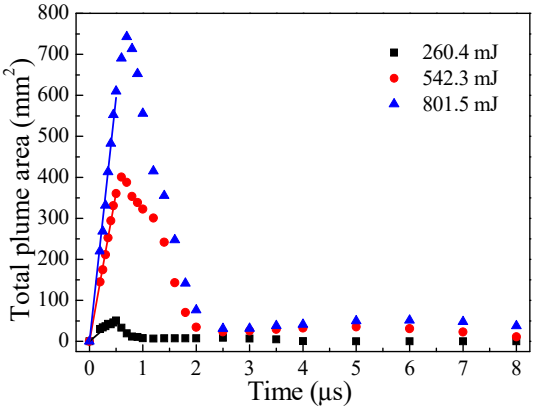

Figure 16. The total plume area variation with time and the linear fitting of initial plume total area at different energies (ambient pressure 0.005 Pa and 26.5% Al).

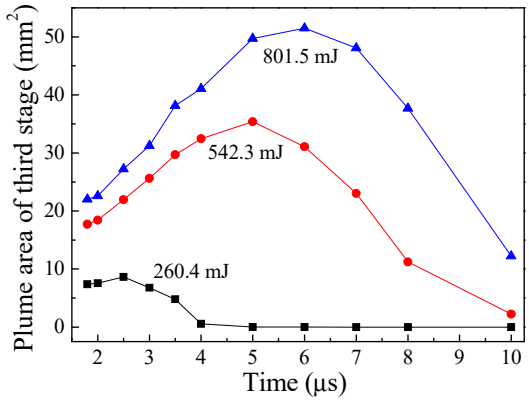

Figure 17. The plume area of third stage variation with time at different laser energies (ambient pressure 0.005 Pa and 26.5% Al).

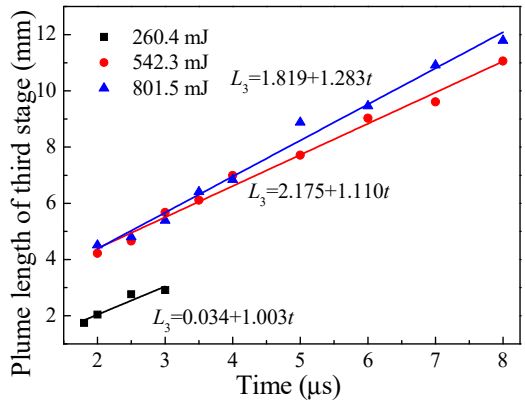

Figure 18. The plume length of third stage variation with time and its linear fitting at different laser energies (ambient pressure 0.005 Pa and 26.5% Al).

3.4. The Effect of Ambient Pressure

The plasma plume evolution process of 26.5% Al at background pressure of 5 Pa and laser energy of 542.3 mJ is shown in Figure 19. Compared with the plume expansion process at 0.005 Pa, the overall process has certain similarity that the plume expansion process contains three stages. As can be seen from the comparison of the plume images, the part with the greater difference is the first stage plume, so the plume image of the first stage plume is emphasized in Figure 19.

Comparing the initial images of plume expansion (0.05 μs~0.15 μs) in Figures 5 and 19, it can be seen that the shape and development of the plume are similar under the two ambient pressures which

is because the internal pressure of the plasma is much higher than the ambient pressure and the plume expansion is almost unaffected by the ambient pressure.

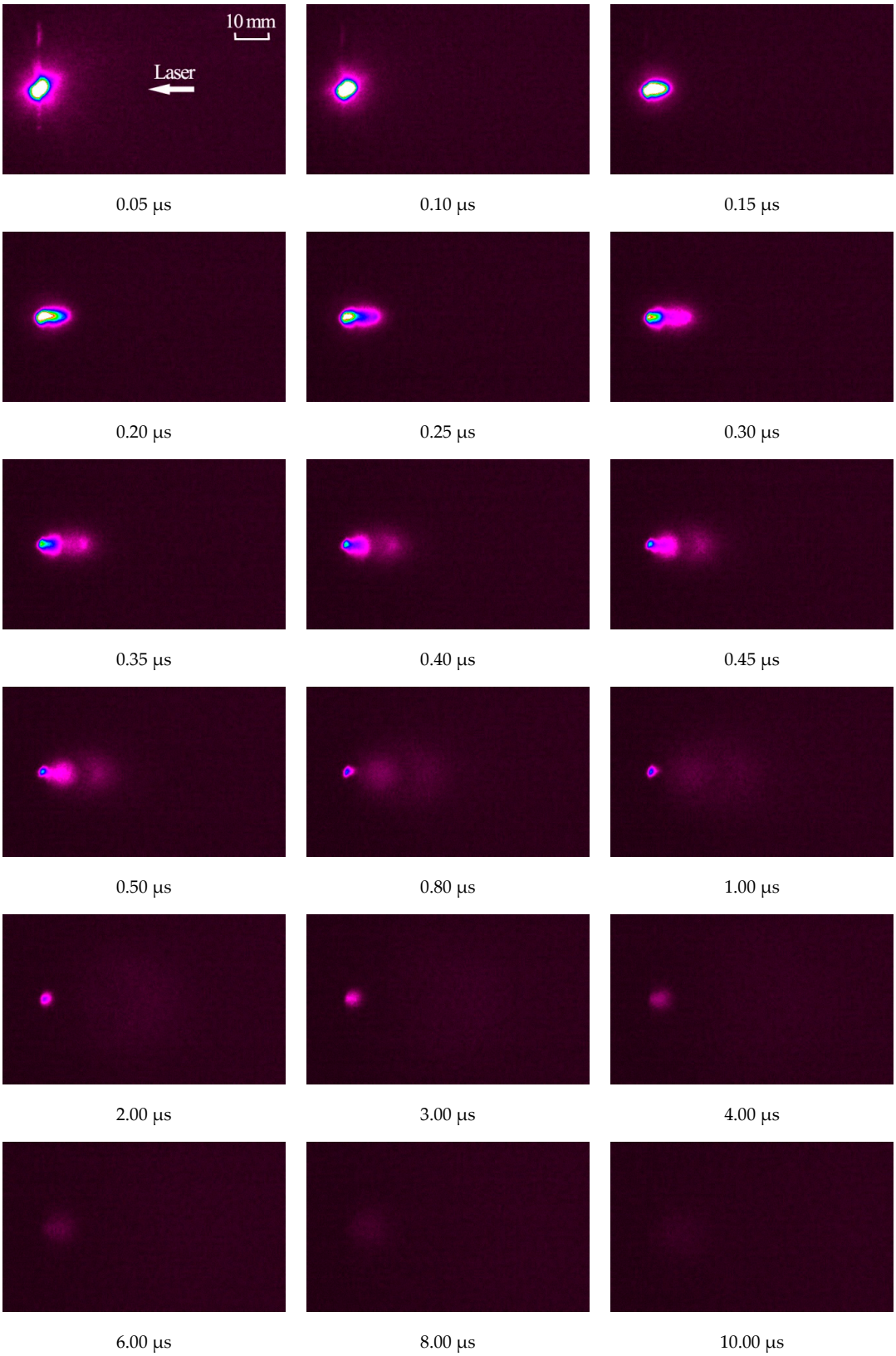

Figure 19. The plasma plume evolution process of 26.5% Al at ambient pressure 5 Pa and laser energy 542.3 mJ.

In the time of 0.20 μs~0.35 μs, the interaction between the plume front and the ambient gas at the ambient pressure of 5 Pa gradually increases and the visible edge at the contact front between the plasma plume and the ambient gas decelerating gradually indicates that the shock wave has been formed [28]. The plasma plume and the ambient gas undergo energy exchange due to ion-ion Coulomb scattering, ion-neutral particle collision and charge exchange interactions [30] at the ambient pressure of 5 Pa, which causes the area of the core highlight region of the plasma plume (the white part of the plume) to drop rapidly and the core highlight region is no longer visible after 0.30 μs, while the core highlight region can still be seen at 1.00 μs when the ambient pressure is 0.005 Pa. At the same time, the rapid decrease of plasma plume brightness also leads to the advance of the separation time of the first stage plume and the second stage plume which is from 0.60 μs at 0.005 Pa to 0.35 μs at 5 Pa. Due to the limiting effect of the ambient gas, the lateral distance and vertical distance of the plasma plume both reduce at the ambient pressure of 5 Pa. Therefore, compared with the ambient pressure of 0.005 Pa, when the ambient pressure is 5 Pa, the overall light intensity of the plasma plume is weaker, the size is smaller and the existence time is shorter.At ambient pressure of 5 Pa, the plume length of first stage variations with time at different energies are shown in Figure 20. At the same laser energy (542.3 mJ), comparing the length of the plume front under the ambient pressure of 0.005 Pa and 5 Pa shows that the length of the plume at the ambient pressure of 5 Pa is less than 0.005 Pa, and the difference between the two plume length increases with the increase of time. The mean free path of gas molecules under the two ambient pressures is inversely proportional to the pressure when the ambient temperature is the same. The mean free path in undisturbed air is $5.36 \times 10^{-3}/P_0$ cm, where P_0 is in Torr [31]. Therefore, the mean free path is about 1.43 m when the ambient pressure is 0.005 Pa, which is 1000 times of that when the ambient pressure is 5 Pa (about 1.43 mm). When the ambient pressure is 0.005 Pa, the characteristic length of the plasma plume is smaller than the mean free path of the ambient gas and the expansion of the plume is almost free expansion. When the ambient pressure is 5 Pa, the initial pressure of the plume is much higher than the ambient pressure, so the expansion of the plume is also similar to free expansion initially. However, when the plume expansion distance is longer than the mean free path, the particles in the plume will collide with the particles in the ambient gas. The plume acts like a piston on the surrounding ambient gas and the ambient gas is gradually compressed which causes the pressure of the ambient gas at the edge of the plume front to be increased [23]. At the same time, the expansion of the plume will cause its own pressure decrease which leads to the decrease of the pressure difference between the plume and the ambient gas, so the expansion velocity of the plume gradually decreases which leads to the difference between the two plume length increases with the increase of time.

The phenomenon that laser plasma plume will form shock waves when it expands in a certain background pressure has been widely studied [32]. The relationship between the front position and time is often described by Sedov-Taylor (S-T) theory which is used to describe the shock wave motion in the ambient gas caused by the energy released by the explosion. The expression of S-T theory [32] is:

$$L_p = 1.08\left(\frac{\gamma+1}{2}\right)^{\frac{2}{2+n}}\left(\frac{E_s}{\rho_0}\right)^{\frac{1}{2+n}} t^{\frac{2}{2+n}} \quad (1)$$

where L_p is the length of plume front, γ is specific heat ratio, E_s is the energy released in the explosion, ρ_0 is the density of the ambient gas, and n = 1, 2, or 3 for planar, cylindrical or spherical shock expansion. The formula (1) can be rewritten as $L_p = a_e t^{2/(n+2)}$. Because the experimental environment is the same under different energies, the ambient pressure and specific heat ratio are the same, and a_e and E_s are positively correlated. The fitting curves of the plasma plume length are shown by the solid line in Figure 20 and their corresponding fitting formulas are written next to the solid line. It can be obtained by calculation that the values of n are 2.338, 0.805 and 0.801 when the laser energies are 260.4 mJ, 542.3 mJ and 801.5 mJ, respectively, which indicates that the shock wave generated by the laser energy of 260.4 mJ is closer to the cylindrical shock and the shock waves generated by the laser energy of

542.3 mJ and 801.5 mJ are closer to the planar shock. Meanwhile, the value of a_e increases with the increase of laser energy and this trend is also consistent with S-T theory.

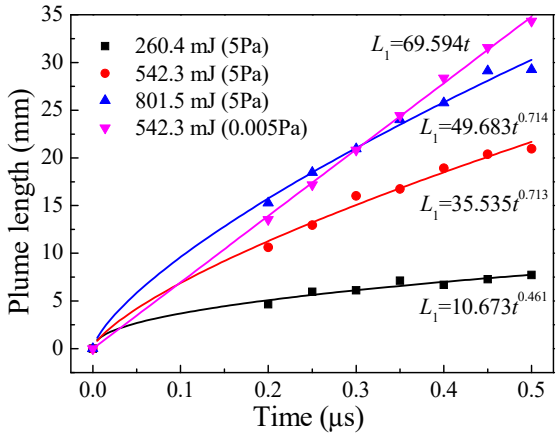

Figure 20. The plume length of first stage variation with time and its fitting curve at different energies (ambient pressure 5 Pa and 26.5% Al).

At ambient pressure of 5 Pa, the total plume area variation with time at different energies is shown in Figure 21. It can be seen from the figure that the total plume area increases with the increase of laser energy. At the same laser energy (542.3 mJ), the total area of the plume under the ambient pressure of 5 Pa is much lower than 0.005 Pa. This is because the limiting effect on the plume is strengthened at the high ambient pressure which causes the area of plume diffusion to decrease.

At ambient pressure of 5 Pa, the total area of initial plume variation with time at different energies is shown in Figure 22. It can be seen from the figure that the change trend of the total area of the initial plume is the same: with the increase of time, the total area of the initial plume increases but the increase rate gradually decreases and tends to a stable value. In order to fit this trend, a formula similar to the drag model [33] is defined. The formula is as follows:

$$S_p = S_{\max}(1 - e^{-\beta t}) \tag{2}$$

where S_p is the plume area, $S_{\max}$ is the maximum area of plume expansion, and β is the drag coefficient. Using Equation (2) to fit the experimental data obtained under ambient pressure of 5 Pa, the results are shown by the solid line in Figure 22 and the corresponding fitting formulas are written next to the solid line. It can be seen from the figure that the maximum area of plume expansion increases with the increase of laser energy, while the drag coefficient decreases.

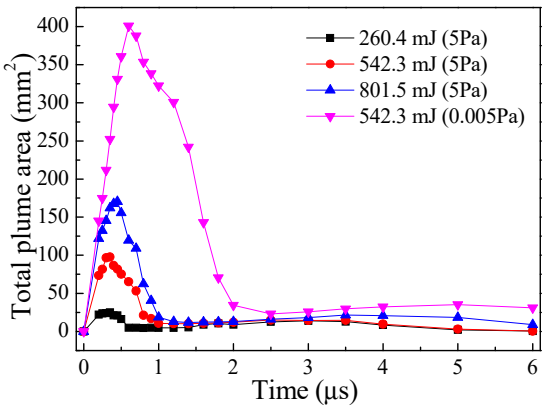

Figure 21. The total plume area variation with time at different energies (ambient pressure 5 Pa and 26.5% Al).

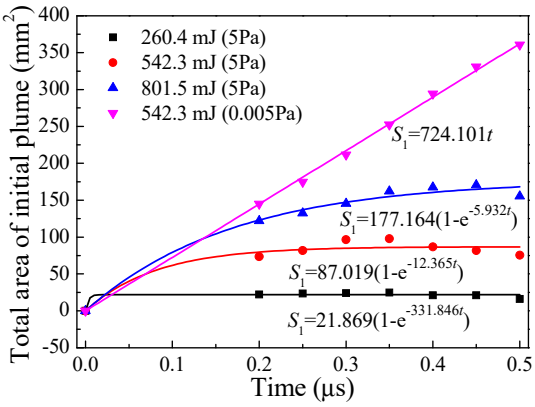

Figure 22. The total area of initial plume variation with time and its fitting curve at different laser energies (ambient pressure 5 Pa and 26.5% Al).

At ambient pressure of 5 Pa, the plume area and plume length of third stage variation with time at different energies are shown in Figures 23 and 24, respectively. It can be seen from the figures that the maximum plume area and the expansion velocity of the third stage plume both increase with the increase of the laser energy. At the same laser energy (542.3 mJ), the plume maximum plume area and the expansion velocity of the third stage plume both decrease with the increase of the ambient pressure, which is due to the limiting effect of the ambient pressure on the third stage plume.

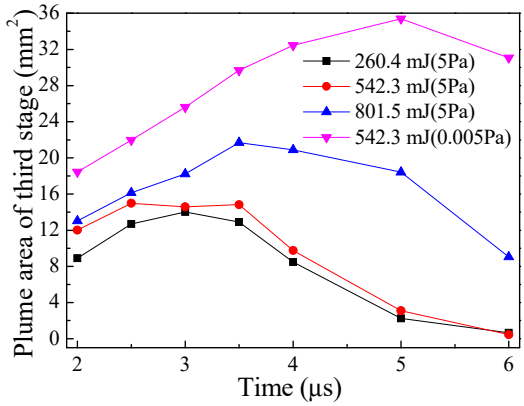

Figure 23. The plume area of third stage variation with time at different laser energies (ambient pressure 5 Pa and 26.5% Al).

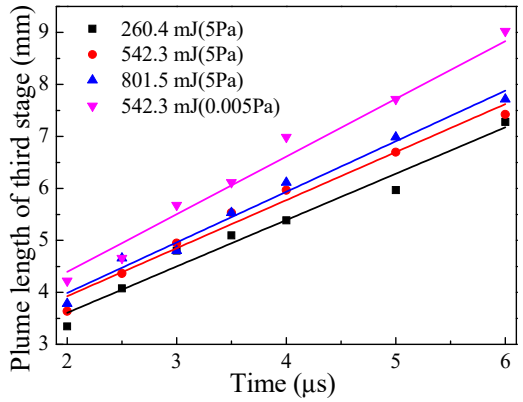

Figure 24. The plume length of third stage variation with time and its linear fitting at different laser energies (ambient pressure 5 Pa and 26.5% Al).

Aiming at the special three-stage plume structure produced by laser ablation of Al/PTFE, time-resolved optical emission spectroscopy [34,35] will be used in the next step to study the composition, electron temperature, and number density of different stages of plume development. At the same time, we also consider using a substrate to collect laser plasma plumes to study the stoichiometry, particle distribution, product composition and distribution [36,37], etc., to further deepen the understanding of laser ablation of Al/PTFE.

The discharge process of MLAPPT is similar to PPT, which can be equivalent to LRC underdamped decay oscillating discharge, and its discharge current gradually oscillates and decay with time. Since the electromagnetic acceleration force generated by MLAPPT is proportional to the square of the discharge current, its electromagnetic acceleration force will also oscillate and decays gradually over time. The three-stage plume structure produced by laser ablation of Al/PTFE will cause the plasma to enter the discharge acceleration channel at different times, which causes the faster laser plasma to enter the discharge acceleration channel first and be accelerated by a large electromagnetic acceleration force, and then the subsequent entry of the laser plasma is accelerated by a smaller electromagnetic acceleration force. This may lead to a greater velocity difference after the plasma is ejected from the discharge acceleration channel, and eventually the plasma plume may present a different stage plume structure similar to that of the laser plasma, which will be verified in subsequent work.

4. Conclusions

By using fast photography, the plasma plume expansion dynamics of laser ablating Al/PTFE is studied. The main conclusions are summarized as follows:

(1) There are three different stage plumes in the plasma plume expansion process of laser ablating Al/PTFE. This phenomenon is different from laser ablating pure Al [30,31] or PTFE [31] and it has not yet been reported in the literature, which is a new ablation phenomenon.

(2) The Al powder doped in PTFE will block part of the laser transmission into the propellant, thus reducing the laser absorption depth of the propellant. Therefore, the laser energy absorption of the propellant has a tendency to change from volume absorption to surface absorption.

(3) The expansion velocity of the first stage plume increases with the increase of Al proportion. The expansion velocity and the total area of the third stage plume increase first and then decrease with the increase of Al proportion, and the maximum value is obtained at 30% Al which indicates that the reaction rate between Al and PTFE is optimal when the reductant is slightly higher than the oxidant in the case of short pulse laser ablation.

(4) As the laser energy increases, the light intensity of the plasma becomes stronger, the plasma size becomes larger and the existence time of plasma becomes longer.

(5) The first stage plume expands freely at the ambient pressure of 0.005 Pa and the plume expansion distance is linearly related to time. The shock wave formed at the interface between the first stage plume front and the ambient gas and the expansion can be described by S-T theory at the ambient pressure of 5 Pa. Compared with the ambient pressure of 0.005 Pa, when the ambient pressure is 5 Pa, the overall light intensity of the plasma plume is weaker, the size is smaller and the existence time is shorter.

Author Contributions: S.T. designed the preparation process of propellant, S.T. and M.W. jointly carried out the preparation experiment of propellant. S.T., Y.Z. and J.L. carried out the laser ablation experiment, J.W. and S.T. analyzed the experimental results. S.T. wrote the manuscript; J.W. and M.W. revised the manuscript. All authors have read and agreed to the published version of the manuscript.

Funding: This research was funded by National Natural Science Foundation of China (Grant number 11772354).

Conflicts of Interest: The authors declare no conflict of interest.

References

1. Kawakami, M.; Lin, W.W.; Igari, A.; Horisawa, H.; Kimura, I. Plasma behaviors in a laser-assisted plasma thruster. In Proceedings of the 39th AIAA/ASME/SAE/ASEE Joint Propulsion Conference and Exhibit, Huntsville, AL, USA, 20–23 July 2003; pp. 1–9.
2. Horisawa, H.; Igari, A.; Kawakami, M.; Kimura, I. Discharge characteristics of laser-electric hybrid thrusters. In Proceedings of the 40th AIAA/ASME/SAE/ASEE Joint Propulsion Conference and Exhibit, Fort Lauderdale, FL, USA, 11–14 July 2004; pp. 1–11.
3. Ayabe, T.; Horisawa, H.; Funaki, I.; Kimura, I. Rectangular laser-electromagnetic hybrid pulsed plasma thruster. In Proceedings of the 30th International Electric Propulsion Conference, Florence, Italy, 17–20 September 2007; pp. 1–7.
4. Horisawa, H.; Mashima, Y.; Yamada, O.; Funaki, I. High I_{sp} mechanism of rectangular laser-electromagnetic hybrid acceleration thruster. In Proceedings of the 32nd International Electric Propulsion Conference, Wiesbaden, Germany, 11–15 September 2011; pp. 1–9.
5. Oigawa, Y.; Horisawa, H.; Funaki, I. Improvement of laser electromagnetic hybrid thruster. In Proceedings of the 33st International Electric Propulsion Conference, Washington, DC, USA, 6–10 October 2013; pp. 1–14.
6. Zhu, C.; Jin, X.; Zhang, Z.W.; Li, N.L. Design and test of a laser assisted pulsed plasma thruster prototype. *IOP Conf. Ser. Earth Environ. Sci.* **2019**, *300*, 042074. [CrossRef]
7. Zhang, D.X.; Zhang, R.; He, Z.; Zhang, F.; Wu, J.J. Discharge characteristics of a laser-electromagnetic coupling plasma thruster for spacecraft propulsion. *Appl. Mech. Mater.* **2012**, *232*, 337–341. [CrossRef]
8. Zhang, D.X. Theoretical, Experimental and Numerical Investigations on a Novel Laser Sustained Pulsed Plasma Thruster. Ph.D. Thesis, National University of Defense Technology, Changsha, China, 2014. (In Chinese)
9. Sinko, J.E.; Pakhomov, A.V.; Millen, S.; Zhu, J.; Sinko, R.J.; Potts, K. Delrin® for propulsion with CO_2 laser: Carbon doping effects. *AIP Conf. Proc.* **2008**, *997*, 254–265. [CrossRef]
10. Schall, W.O.; Tegel, J.; Eckel, H.A. Ablation performance experiments with metal seeded polymers. *AIP Conf. Proc.* **2005**, *766*, 423. [CrossRef]
11. Phipps, C.; Birkan, M.; Bohn, W.; Eckel, H.A.; Horisawa, H.; Lippert, T.; Michaelis, M.; Rezunkov, Y.; Sasoh, A.; Schall, W.; et al. Review: Laser-ablation propulsion. *J. Propuls. Power* **2010**, *26*, 609–637. [CrossRef]
12. Cheng, J.Z.; Cai, J.; Hu, Y.; Zhang, Z.M.; Ding, Z.J. Experimental study of laser propulsion by using polymer propellant doped with metal powders. *High Power Laser Part. Beams* **2008**, *20*, 1190–1194. (In Chinese)
13. Peng, J.; Zheng, H.; Hu, X.J.; Tang, Z.P. Polymer seeded with metallic powders in ablation mode laser propulsion. *High Power Laser Part. Beams* **2009**, *21*, 821–825. (In Chinese)
14. Maesato, H.; Koizumi, E.; Tahara, H. Performance characteristics of low-power laser ablative thrusters for small satellites. *AIP Conf. Proc.* **2006**, *830*, 284. [CrossRef]
15. Burton, R.L.; Turchi, P.J. Pulsed plasma thruster. *J. Propuls. Power* **1998**, *14*, 716–735. [CrossRef]
16. Zhang, Z.; Ling, W.Y.L.; Tang, H.B.; Cao, J.B.; Liu, X.Y.; Wang, N.F. A review of the characterization and optimization of ablative pulsed plasma thrusters. *Rev. Mod. Plasma Phys.* **2019**, *3*, 5. [CrossRef]
17. Zhang, Y.; Zhang, D.X.; Wu, J.J.; He, Z.; Zhang, H. A novel laser ablation plasma thruster with electromagnetic acceleration. *Acta Astronaut.* **2016**, *127*, 438–447. [CrossRef]
18. Zhang, Y.; Zhang, D.X.; Wu, J.J.; Li, J.; He, Z.F. Non-Fourier heat conduction and phase transition in laser ablation of polytetrafluoroethylene (PTFE). *Acta Astronaut.* **2017**, *140*, 338–350. [CrossRef]
19. Schönherr, T.; Abe, Y.; Okamura, K.; Koizumi, H.; Arakawa, Y.; Komurasaki, K. Influence of propellant in the discharge process of PPT. In Proceedings of the 48th AIAA/ASME/SAE/ASEE Joint Propulsion Conference and Exhibit, Atlanta, GA, USA, 30 July–1 August 2012; pp. 1–9.
20. Küper, S.; Stuke, M. Ablation of polytetrafluoroethylene (teflon) with femtosecond UV excimer laser pulses. *Appl. Phys. Lett.* **1989**, *54*, 4–6. [CrossRef]
21. Mitra, A.; Thareja, R.K. Determination of laser ablation threshold of teflon at different harmonics of Nd: YAG laser using photothermal deflection technique. *J. Mater. Sci.* **1999**, *34*, 615–619. [CrossRef]
22. Xu, S.L. Study on the Mechanical Performance of Polytetrafluorethylene/Al Energetic Reactive Materials. Ph.D. Thesis, National University of Defense Technology, Changsha, China, 2010. (In Chinese)
23. Amoruso, S.; Sambri, A.; Wang, X. Propagation dynamics of a $LaMnO_3$ laser ablation plume in an oxygen atmosphere. *J. Appl. Phys.* **2006**, *100*, 013302. [CrossRef]

24. Singh, R.; Narayan, J. Pulsed-laser evaporation technique for deposition of thin films: Physics and theoretical model. *Phys. Rev. B* **1990**, *41*, 8843–8859. [CrossRef] [PubMed]
25. Harilal, S.S.; Bindhu, C.V.; Tillack, M.S.; Najmabadi, F.; Gaeris, A.C. Plume splitting and sharpening in laser-produced aluminium plasma. *J. Phys. D Appl. Phys.* **2002**, *35*, 2935–2938. [CrossRef]
26. Li, G. Research on Propulsion Mechanism and Performance Optimization of Polymer Ablation by Pulsed Laser Irradiation. Ph.D. Thesis, National University of Defense Technology, Changsha, China, 2014. (In Chinese)
27. Enescu, F.; Irimiciuc, S.A.; Cimpoesu, N.; Bedelean, H.; Bulai, G.; Gurlui, S.; Agop, M. Investigations of laser produced plasmas generated by laser ablation on geomaterials. Experimental and theoretical aspects. *Symmetry* **2019**, *11*, 1391. [CrossRef]
28. Abdelli-Messaci, S.; Kerdja, T.; Lafane, S.; Malek, S. Fast imaging of laser-induced plasma emission from a ZnO target. *Spectrochim. Acta Part B At. Spectrosc.* **2009**, *64*, 968–973. [CrossRef]
29. Fikry, M.; Tawfik, W.; Omar, M.M. Investigation on the effects of laser parameters on the plasma profile of copper using picosecond laser induced plasma spectroscopy. *Opt. Quantum Electron.* **2020**, *52*, 249. [CrossRef]
30. Harilal, S.S.; Bindhu, C.V.; Tillack, M.S.; Najmabadi, F.; Gaeris, A.C. Internal structure and expansion dynamics of laser ablation plumes into ambient gases. *J. Appl. Phys.* **2003**, *93*, 2380. [CrossRef]
31. Thareja, R.K.; Misra, A.; Franklin, S.R. Investigation of laser ablated metal and polymer plasmas in ambient gas using fast photography. *Spectrochim. Acta Part B* **1998**, *53*, 1919–1930. [CrossRef]
32. De Posada, E.; Arronte, M.A.; Ponce, L.; Rodriguez, E.; Flores, T.; Lunney, J.G. On the use of shockwave models in laser produced plasma expansion. *J. Phys. Conf. Ser.* **2011**, *274*, 012078. [CrossRef]
33. Phelps, C.; Druffner, C.J.; Perram, G.P.; Biggers, R.R. Shock front dynamics in the pulsed laser deposition of $YBa_2Cu_3O_{7-x}$. *J. Phys. D Appl. Phys.* **2007**, *40*, 4447–4453. [CrossRef]
34. Shaikh, N.M.; Hafeez, S.; Rashid, B.; Mahmood, S.; Baig, M.A. Optical emission studies of the mercury plasma generated by the fundamental, second and third harmonics of a Nd: YAG laser. *J. Phys. D Appl. Phys.* **2006**, *39*, 4377–4385. [CrossRef]
35. Chen, A.; Jiang, Y.; Wang, T.; Shao, J.; Jin, M. Comparison of plasma temperature and electron density on nanosecond laser ablation of Cu and nano-Cu. *Phys. Plasma* **2015**, *22*, 033301. [CrossRef]
36. Arnold, C.B.; Aziz, M.J. Stoichiometry issues in pulsed-laser deposition of alloys grown from multicomponent targets. *Appl. Phys. A* **1999**, *69*, S23–S27. [CrossRef]
37. Vitug, J.D.R.; Vero, J.C.D.; Blanca, G.R.S.; Sarmago, R.V.; Garcia, W.O. Stoichiometric transfer by infrared pulsed laser deposition of Y-doped Bi–Sr–Ca–Cu–O investigated using time-resolved optical emission spectroscopy. *J. Appl. Spectrosc.* **2012**, *78*, 855–860. [CrossRef]

© 2020 by the authors. Licensee MDPI, Basel, Switzerland. This article is an open access article distributed under the terms and conditions of the Creative Commons Attribution (CC BY) license (http://creativecommons.org/licenses/by/4.0/).